ADVANCED HEALTHCARE MATERIALS
www.advhealthmat.de

Ultrastretchable Kirigami Bioprobes

*Yusuke Morikawa, Shota Yamagiwa, Hirohito Sawahata, Rika Numano, Kowa Koida, Makoto Ishida, and Takeshi Kawano**

An ultrastretchable film device is developed that can follow the shape of spherical and large deformable biological samples such as heart and brain tissues. Although the film is composed of biocompatible parylene for the device substrate and metal layers of platinum (Pt)/titanium (Ti), which are unstretchable materials, the film shows a high stretchability by patterning slits as a "Kirigami" design. A Pt/Ti-microelectrode array embedded in 11 µm thick parylene film with 5 × 91 slits exhibits a film strain of ≈250% at 9 mN strain-force (0.08 MPa in stress) with a Young's modulus of 23 kPa, while the 3 × 91-slit film shows a Young's modulus of 3.6 kPa. The maximum strains of these devices are ≈470% and ≈840%, respectively. It is demonstrated that the Kirigami-based microelectrode device can simultaneously record in vivo electrocorticogram signals from the visual and barrel cortices of a mouse by stretching the film and tuning the electrode gap. Moreover, wrapping the Kirigami device around a beating mouse's heart, which shows large and rapid changes in the volume and the surface area, can record the in vivo epicardial electrocardiogram signals. Such a small Young's modulus for a stretchable device reduces the device's strain-force, minimizing the device-induced stress to soft biological tissues.

High stretchability and deformability are promising properties to expand the applications of flexible film (or "sheet") electronics, including sensors, actuators, and energy harvesters.[1–3] In particular, they have great potential for 3D-shaped soft biological samples such as organs and tissues. These biological samples have relatively small Young's moduli of 1 kPa for brain tissue and 10 kPa for heart (as a muscle).[4] Additionally, the volume and surface of the heart show large and rapid changes. Assuming an ontogenetic process and pathological hypertrophy/atrophy, the deformation of brain tissue exceeds 300%.[5]

However, conventional elastomer-based devices require a large strain-force [e.g., ≈100% strain at 0.73 MPa for polydimethylsiloxane (PDMS)[6]] due to the material Young's modulus (0.73 MPa for PDMS[6]). For device applications to soft biological samples, it is important to reduce the Young's modulus of these stretchable devices in order to decrease the device-induced stress to the tissue for low invasiveness and safer measurements compared to conventional stretchable devices. In addition, the strains of conventional devices are limited by the elasticity of the device substrate and the interconnections [e.g., silver flakes and self-similar geometry interconnections show remarkable stretchabilities of 215%[2] and 300%,[3] respectively].

In the Japanese culture, "Origami" (ori means "folding" and gami means "paper")[7] and "Kirigami" (kiri means "cutting") are artistic transformations from a flat sheet/film into numerous 2D and 3D sculptures through folding, cutting, and gluing techniques. Kirigami designs have been used in material science and engineering to prepare ultrastretchable 2D materials, including graphene[8] and nanocomposites.[9] The remarkable feature of Kirigami is that rigid and unstretchable materials can be rendered stretchable compared to other elastomer-based stretchable materials (e.g., 370% strain for nanocomposites[9]). This is a way to realize stretchable electronics by utilizing rigid and unstretchable materials, including insulators, metals, and semiconducting materials.

In this study, we present a Kirigami-based flexible bioprobe film device. The device consists of a multiple layered system composed of unstretchable materials: insulating parylene-C (Young's modulus 2.8 GPa and yield strain ≈3%) for the device substrate and platinum (Pt) (Young's modulus 168 GPa) with titanium (Ti) adhesion (Young's modulus 116 GPa) for the electrode layer embedded in the parylene. This device realizes multichannel biological signal recordings with the device's highly stretchable and deformable properties.

Origami and Kirigami may realize numerous 2D (e.g., stretching) and 3D devices at the nano/microscale. Similar to how Origami paper (120 mm × 160 mm) can be stretched by cutting a slit pattern with scissors (**Figure 1**a,b), the parylene-C

Y. Morikawa, Dr. S. Yamagiwa, Prof. H. Sawahata, Prof. M. Ishida, Prof. T. Kawano
Department of Electrical and Electronic Information Engineering
Toyohashi University of Technology
1-1 Hibarigaoka Tempaku-cho, Toyohashi 441-8580, Japan
E-mail: kawano@ee.tut.ac.jp
Prof. R. Numano, Prof. K. Koida, Prof. M. Ishida
Electronics-Interdisciplinary Research Institute (EIIRIS)
Toyohashi University of Technology
1-1 Hibarigaoka Tempaku-cho, Toyohashi 441-8580, Japan
Prof. R. Numano
Department of Environmental and Life Sciences
Toyohashi University of Technology
1-1 Hibarigaoka Tempaku-cho, Toyohashi 441-8580, Japan
Prof. K. Koida
Department of Computer Science and Engineering
Toyohashi University of Technology
1-1 Hibarigaoka Tempaku-cho, Toyohashi 441-8580, Japan

DOI: 10.1002/adhm.201701100

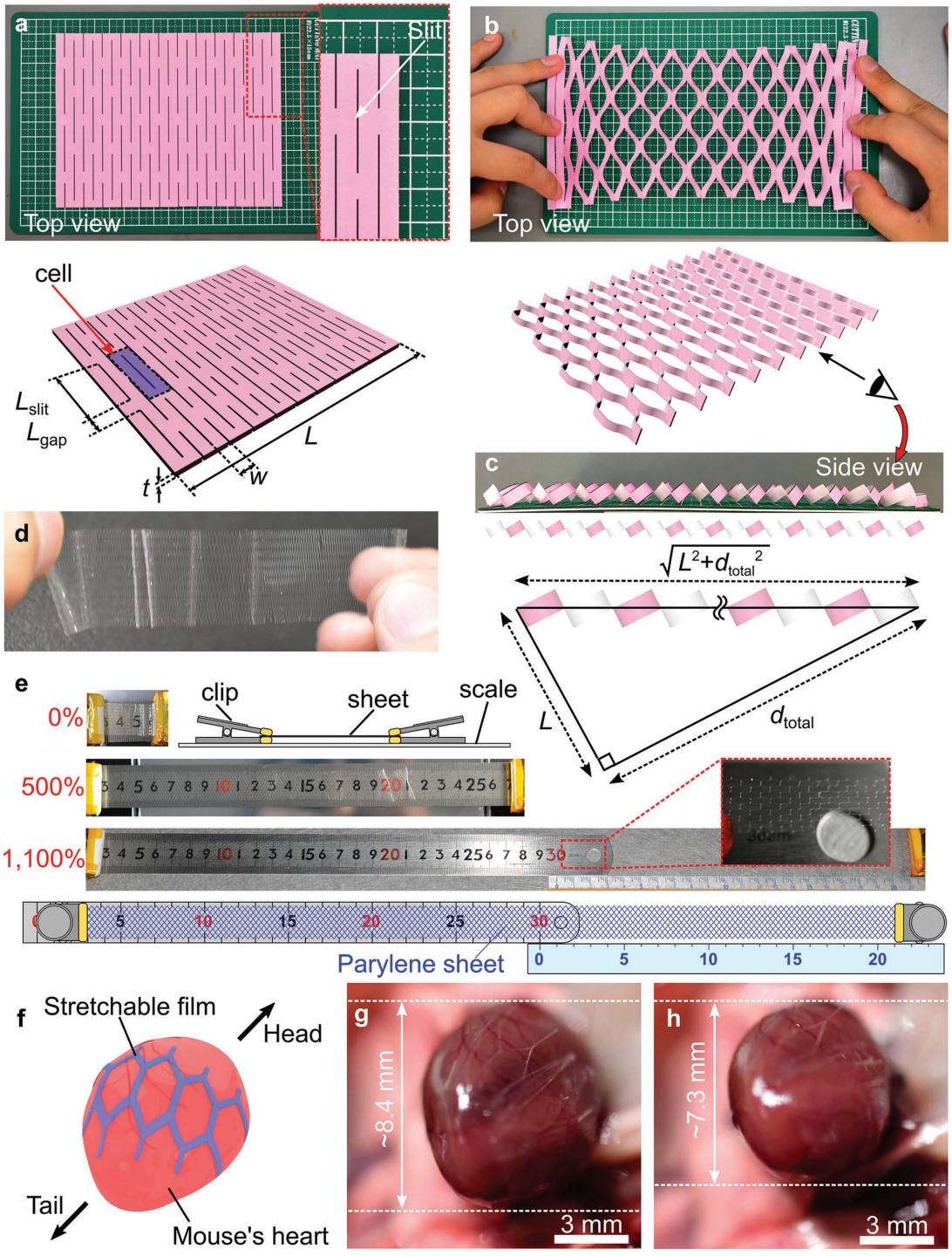

Figure 1. "Kirigami" design-based parylene film. a,b) Photographs and schematics of stretching of a "Kirigami" paper (120 mm × 160 mm) with a slit pattern formed by scissors (a: before and b: after stretching). Schematic of "before stretching" (a) includes a cell unit (purple colored), which is used in the modeling. c) Accurate displacement of the stretched film by considering the Pythagorean theorem. d) Photograph of the fabricated Kirigami parylene film (40 mm long, 20 mm wide, and 10 μm thick) consisting of an array of 5 × 361 slits (N_r = 5, N_c = 180) (Movie S1 of the Supporting Information shows repeated stretching of the film). e) Quantitative analysis of the stretchability of a fabricated parylene film. The film, which consists of 5 × 361 slits (N_r = 5, N_c = 180), is stretched over a 30 cm ruler with two clips. The film exhibits a stretchability of 1100%, which is measured with an additional ruler. f–h) Schematic and photographs of a fabricated parylene film placed over a beating mouse heart. The film with one row design (N_r = 1) follows the heart pulsation (also see Movie S2 of the Supporting Information).

film's stretching mechanism is based on the out-of-plane bending of the membranes around each slit. Namely, the bending property of the membranes dominates the stretchability of the whole film system. Compared to in-plane bending of membranes,[10] the out-of-plane bending mechanism realizes a larger strain at the same strain-force. Based on the traditional Kirigami concept, herein highly stretchable and deformable bioprobe film devices are fabricated. Such Kirigami films can be realized by patterning micro/nanoscale slits in the film using conventional patterning processes [e.g., photolithography technique]. One advantage of the Kirigami concept is that this technique is applicable not only to stretchable materials but also to other bendable (unstretchable) materials.

A beam model can be used to discuss the stretching property of a Kirigami film with a slit design.[9] For simplicity, herein we use a cell unit consisting of a slit and four beams around the slit (purple colored section in Figure 1a). The design of the cell unit array (row and column numbers of cell units) defines the stretching property of the whole film system. Without considering the out-of-plane bending of each beam with a rotation, the film displacement associated with beam bending, d_{total}(d_{total} in Figure 1c), is proportional to the total load, P, of the film, which is expressed as

$$d_{\text{total}} = \frac{N_c}{N_r}\frac{P(L_{\text{slit}} - L_{\text{gap}})^3}{8Ewt^3} \quad (1)$$

where N_r and N_c are the row and the column numbers of the cell units, respectively. E, w, and t are Young's modulus, the beam width, and film thickness, respectively. L_{slit} and L_{gap} are the slit length and the gap between the slits, respectively (Figure 1a). This formula suggests that the stretching property of the film is proportional to the column-/row-numbers ratio (N_c/N_r), while the bending property of each beam contributes to the film stretchability. The bending property of each beam is defined by the material properties (e.g., Young's modulus) and geometry (e.g., length, width, and thickness) of the membrane. For a more accurate expression considering the rotation of each beam, the displacement of the film, $d_{\text{total, actual}}$, is given by the Pythagorean theorem (Figure 1c) as

$$d_{\text{total, actual}} = \sqrt{L^2 + d_{\text{total}}^2} - L \quad (2)$$

where L is the film length prior to stretching. Herein we use the actual displacement of the film, $d_{\text{total, actual}}$, for the film stretching tests and to discuss the stretching properties.

We demonstrate that parylene-C produces a flexible film that is highly stretchable and deformable. The fabrication process is based on simple steps. First, the parylene film is deposited on a substrate (e.g., silicon wafer). Second the slit array is patterned. Third, the parylene film is peeled from the substrate.

A 10 µm thick parylene-C film was deposited on a silicon substrate. To form the slit patterns, the parylene-C film was etched by oxygen (O_2) plasma with a slit mask of Ti (≈80 nm thick), which was patterned by a tetrafluoromethane (CF_4) plasma with a photoresist prior to parylene etching (Figure S3 of the Supporting Information shows the process steps). After removing the Ti mask (CF_4 plasma), the parylene film was released from the silicon substrate with ethanol. The fabricated parylene-C film, which measures 40 mm long, 20 mm wide, and 10 µm thick, consists of an array with 5 × 361 slits (N_r = 5, N_c = 180) (Figure 1d) (Movie S1 of the Supporting Information shows repeated film stretching.) Herein the designed slit length (L_{slit}) and the gap between the slits (L_{gap}) are 3400 and 600 µm, respectively, while the beam width (w) is ≈100 µm. This design results in a 1400 µm long and 100 µm wide parylene membrane surrounding each slit. To avoid the stress concentration at the edge of each slit, a circular-shaped edge design was used.[9] Compared to the corner-shaped edge, the circular-shaped edge with a 20 µm diameter shows approximately two times less stress at the edge (simulation results, Figure S5 of the Supporting Information), making the film unbreakable while stretching.

The fabricated parylene film exhibits a great stretching property, as demonstrated in the quantitative analysis (Figure 1e). The initial 40 mm long parylene film can be stretched 1100% to a length of 480 mm before the film breaks. As a preliminary test, a Kirigami film with a one-row design was mounted on a beating mouse heart, whose volume and surface area rapidly change (Figure 1f–h; Movie S2 of the Supporting Information).

To compare the stretchability of the slit-designed Kirigami film, we also fabricated another type of parylene film with a "diamond mesh" design (Figure S7 of the Supporting Information). Because there are fewer meshes (or fewer bendable beams) in the same film geometry (40 mm long, 20 mm wide, and 10 µm thick), the stretchability of the meshed parylene film is limited to 55 mm (≈83%) before the film breaks (Figure S7 of the Supporting Information), indicating that the proposed slit-array design (Figure 1) is suitable to obtain films with large stretchabilities.

Figure 2a shows the fabrication process of the proposed Kirigami-based bioprobe device, which consists of an array of microscale planar electrodes for multisite recording of biological signals. The device fabrication was the same as the parylene film process (Figure S3 of the Supporting Information), except that electrodes were embedded in the film.[11,12] For the device bottom layer, a 5 µm thick parylene-C film was deposited on a silicon substrate. As the electrode layer, Pt with an adhesion layer of Ti (40 nm thick for Pt and 60 nm thick for Ti) was sputtered over the bottom parylene layer and subsequently patterned by plasma etchings (argon for Pt and CF_4 for Ti). Then a 5 µm thick parylene-C film was deposited over the electrode-/bottom parylene-layers for the device top layer. Both the top and the bottom parylene layers were patterned by O_2 plasma with a Ti mask. After removing the Ti mask, the parylene device was released from the silicon substrate with ethanol (Figure 2b) (Figure 2c shows batch-processed devices on a silicon substrate). The fabricated 5 × 91 slits (N_r = 5, N_c = 45) designed bioprobe film device has a 1600 µm slit length (L_{slit}), 400 µm gap between the slits (L_{gap}), and 100 µm beam width (w). The other film type with 3 × 91 slits (N_r = 3, N_c = 45) results in a different beam design (L_{slit} = 2700 µm, L_{gap} = 600 µm, same w = 100 µm). Each recording site of 50 µm diameter Pt electrode is connected with a Pt-interconnection (20 µm wide), which zigzags on a single beam (w = 100 µm) (Figure 2d). Figure 2f shows the other type of interconnection design where three interconnections are designed in a single beam (w = 100 µm). For in vivo recording applications, the fabricated film device was packaged with a polyimide-based flexible

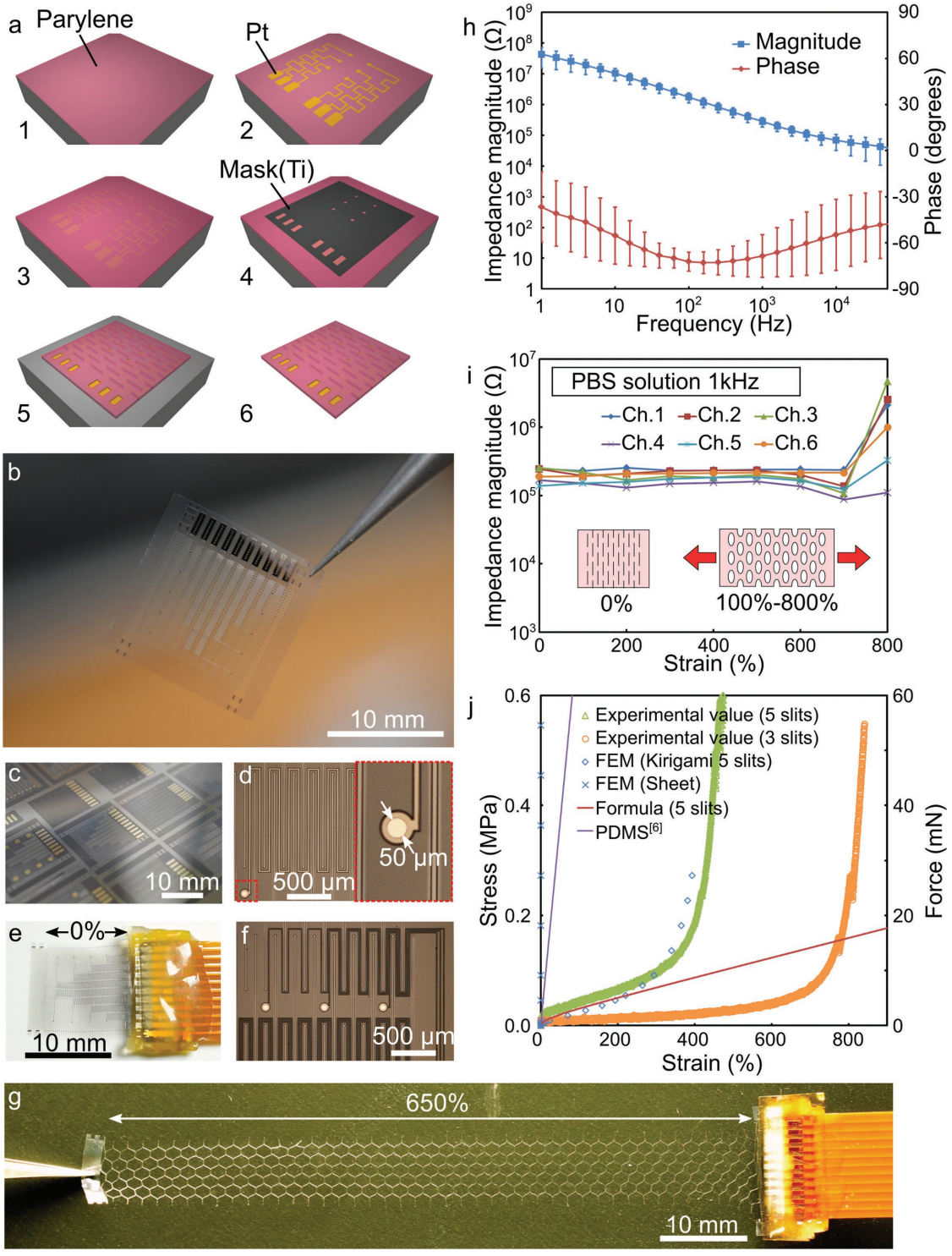

Figure 2. Kirigami-based highly stretchable and flexible bioprobe devices. a) Device fabrication steps: (1) deposition of the bottom layer of parylene-C on a silicon substrate, (2) sputtering of a Pt-electrode layer with a Ti adhesion layer over the parylene layer and subsequent plasma etching to form a pattern, (3) deposition of the device top layer of parylene-C over the Pt-electrode layer and the bottom parylene layer, (4) sputtering of a hard mask of Ti over the top parylene layer and plasma-etching patterning, (5) patterning of the both top and bottom parylene layers by a plasma with the Ti mask, and then removal of the Ti mask, and (6) release of the parylene device from the silicon substrate with ethanol. b) Photograph of the fabricated device after removing from the silicon substrate. c) Photograph showing batch-processed devices on a silicon substrate. d) Photograph showing the 50 μm diameter planar Pt-electrode site in a device connected with a zigzag Pt-interconnection. e) Photograph of a device packaged with a polyimide-based flexible printed circuit (FPC) for subsequent in vivo applications. f) Photograph showing the other type of interconnection design where three

printed circuit (FPC) (Figure 2e). Figure 2g shows a fabricated device [3 × 91 slits design (N_r = 3, N_c = 45)] stretched 650% by tweezers (also see Movie S3 of the Supporting Information).

The electrolyte/metal interfacial electrical impedance of the Pt electrode was measured in a phosphate-buffered saline (PBS). Without stretching the film device (stretchability = 0%), the magnitude of the Pt-electrode impedance is 311 ± 32 kΩ (mean ± SD) at 1 kHz (Figure 2h). Figure 2i shows the strain-dependent impedance characteristics of the Pt electrodes taken from a film device designed with 3 × 91 slits. The impedance is independent of film stretching between 0% and 500%. In this stretching regime, the electrical properties of the Pt electrodes do not change because each beam (parylene/Pt/parylene layer system) bends. As the film stretches between 600% and 700%, the electrode impedance slightly drops, probably due to the stress-induced peeling of the parylene layer from the Pt layer (e.g., concentrated stress at the beam-edge). However, at 800% film stretching, the electrode impedance increases significantly (>10^6 Ω) prior to the film breaking.

Figure 2j includes the experimentally measured stress (force)–strain curve for a film device designed with 5 × 91 slits (blue squares in Figure 2j). The measurement of the 5 × 91-slit device confirms that a 9 mN strain-force (0.08 MPa in stress) to the film realizes a high film stretchability of ≈250%. In this regime (20–250% strain), the film's strain is proportional to the stress (force) (green triangles in Figure 2j). The Young's modulus taken from the stress–strain curve is 23 kPa, which is ≈32 times lower than that of conventional elastomer-based stretchable devices with PDMS (0.73 MPa for PDMS[6]) (purple line in Figure 2j).

The experimentally obtained slope (20–250% strain) was compared with the values calculated by formula (2) (red line in Figure 2j) and the fit by the finite element method (FEM) (blue squares in Figure 2j) (model appeared in Figure S2 of the Supporting Information). Because the fabricated device shows a parylene thickness of 11 µm (design value is 10 µm), we used the same film thickness in both the formula and the FEM. The difference in the slope between the formula and the experimental values in this regime is 12.2%, except for the difference at the initial strain point (green triangles in Figure 2j). This slope difference is due to device fixation in the measurement, in which each film edge is fixed with a ridged substrate, which limits stretching in some beams (approximately two column cell units). This edge effect is not considered in the formula or the FEM. Further consideration of the in-plane mode in the calculations offer more accurate data fittings. The difference in the initial strain point is due to the in-plane bending-mode phenomenon in the membranes prior to the out-of-plane bending[13] (Both the formula and FEM values are based on the out-of-plane bending mode). In addition, these calculations do not include the metal layer (40 nm thick for Pt, 60 nm thick for Ti). To further analyze the fabricated Kirigami device, we modeled the multiple layered Kirigami system, in which each beam consists of the parylene substrate and the embedded Pt/Ti-metal interconnection (Supporting Information). By considering the metal layer, the slope difference with and without the metal layer is 0.7% (Supporting Information). Because the thickness of the metal layer (Pt/Ti) in the fabricated device is 110 times thinner than the parylene's one (11 µm), there is not a significant slope differences in this regime. At a strain over 250% (an applied force over 9 mN), the film strain becomes saturated due to the limitation of structural deformations.[9,13] Saturation is confirmed in both the experimental and the FEM data. The maximum strain of the device reaches ≈470% at 65 mN (0.59 MPa). The other film device with 3 × 91 slits shows an increased maximum strain of ≈840% at 58 mN (0.53 MPa) [Young's modulus at the linear regime (20–450% strain) is 3.6 kPa] (orange circles, Figure 2j). Figure 2j also includes the calculated stress–strain curve for a parylene film without slits as a comparison (blue crosses, Figure 2j).

One challenge of such highly stretchable, deformable, and flexible bioprobe film devices is neuronal signal recordings from brain tissue, which is soft and has a spherical shape and pulsatile motion in in vivo recordings. Recent advances in microfabrication technology have realized flexible microscale planar electrocorticogram (ECoG) electrode array devices and demonstrated the advantage of conformal wrapping onto brain tissue.[14–16] An additional requirement of such devices is that the electrode array must have design variability, such as application dependent, tunable intervals between electrodes during the measurements. Other requirements include conformal wrapping of an in vivo brain, which shows an increase/decrease in its tissue volume due to pulsation of the brain.

Figure 3a,b shows a fabricated 5 × 91 slits designed Kirigami-based bioprobe device, which consists of 10 channel planar Pt electrodes [50 µm diameter, 311 ± 32 kΩ (mean ± SD) impedance at 1 kHz], demonstrating the advantage of tunable intervals between the electrodes over the cortical surface of a mouse brain in vivo. To realize simultaneous neuronal recordings from the visual cortex (primary visual cortex, V1) and barrel cortex (primary somatosensory cortex barrel field, S1B) of a mouse brain, the positions of the electrodes were aligned with these cortical areas while the gap between the electrodes increased due to film stretching (Figure 3c,d). After positioning the first electrode of Ch. 9 over the V1, the second electrode of Ch. 8 was positioned over the S1B (3 mm away from the V1) by stretching the film and changing the electrode gap from

interconnections are designed in a single parylene-beam (w = 100 µm). g) Photograph showing a fabricated device [3 × 91 slits design (N_r = 3, N_c = 45)] stretched to 650% by tweezers (also see Movie S3 of the Supporting Information). h) Impedance characteristics of the fabricated device measured in PBS without device stretching (0%). Averages and standard deviations of both impedance magnitude and phase characteristics are taken from eight samples; the error bars, SD. i) Strain-dependent impedances of the fabricated device at 1 kHz in PBS. Herein the measured device is a designed film with 3 × 91 slits (N_r = 3, N_c = 45), which is stretched from 0% to 800%. j) Experimentally measured strain-force characteristics of the fabricated device. The measured device is a designed film with 5 × 91 slits (N_r = 5, N_c = 45, green triangles) and 3 × 91 slits (N_r = 3, N_c = 45, orange circles). The graph also includes the calculated value by formulas (1) and (2) (red line) and the FEM simulation [blue squares for with slit (Kirigami) and blue crosses for without slit (sheet)], and strain-force characteristic of PDMS[6] (purple line).

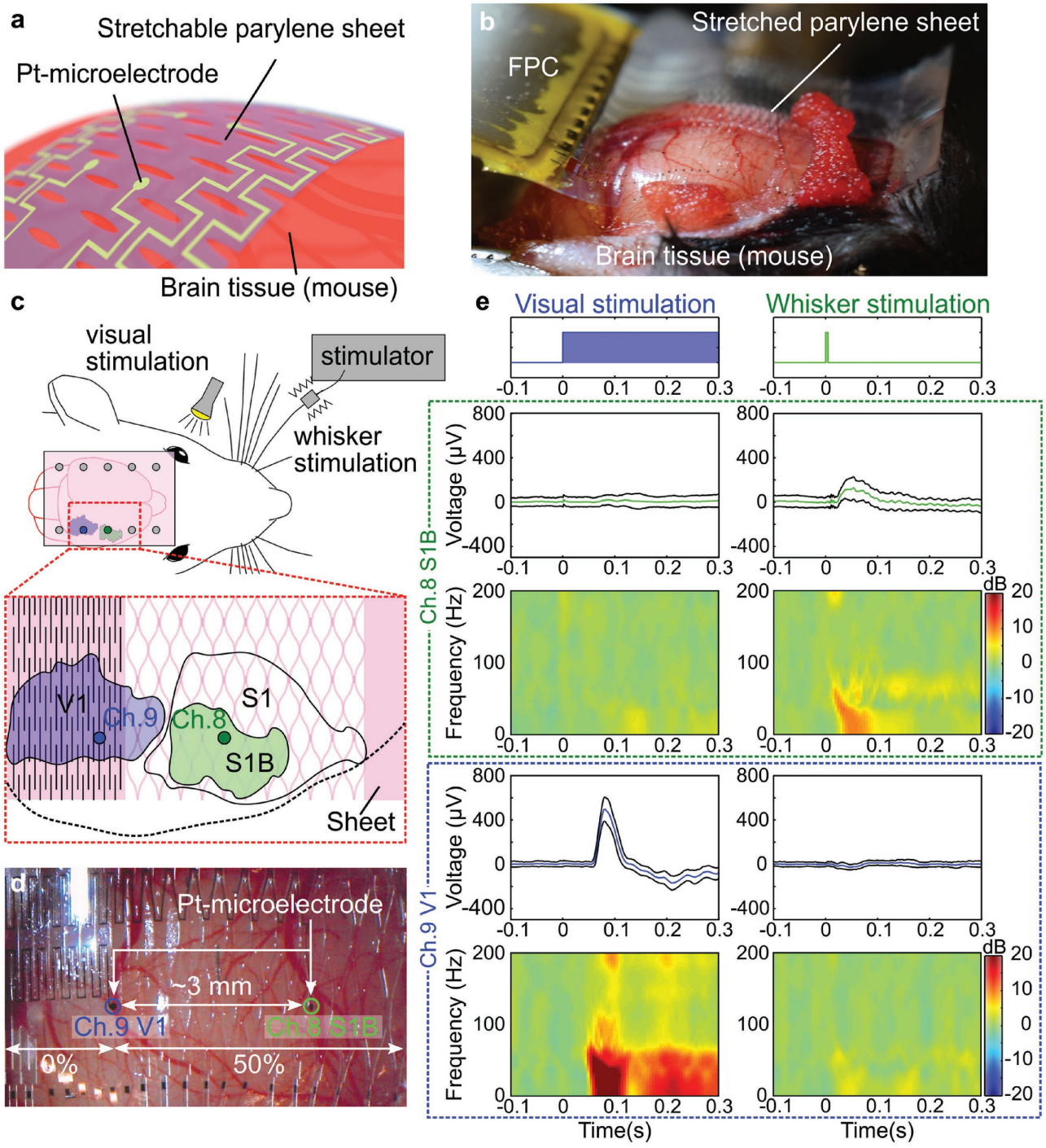

Figure 3. ECoG signal recordings from a mouse brain in vivo. a) Schematic of the Kirigami device placed over mouse brain tissue. b) Photograph showing the fabricated Kirigami-based microscale planar electrode (Pt) array device [5 × 91 slits design ($N_r = 5$, $N_c = 45$)] placed over the cortical surface of a mouse brain in vivo, while the electrode positions are adjusted by stretching the film. c) Illustrations of the animal experiment and the positions of the Pt electrodes. To realize ECoG recordings from the visual (V1) and barrel (S1B) cortices of the mouse brain, the gap between Pt electrodes (Chs. 9 and 8) is changed from 2 mm (initial gap, 0% strain) to ≈3 mm (50% strain) by stretching the film. d) Photograph of the Pt electrodes (Chs. 8 and 9) after the position adjustments, representing the schematic shown in (c). e) Detected ECoG responses using the Pt electrodes during visual and whisker stimuli. Pt electrodes of Chs. 8 and 9 are placed over the barrel (S1B) and visual (V1) areas of the brain cortex, respectively. Each panel includes the waveforms and time-frequency domain plots of the recorded ECoG signals. These neuronal responses were detected by Ch. 8 electrode during whisker stimuli and Ch. 9 electrode during visual stimuli, respectively [paired *t*-test, $n = 100$ trials, $p = 1.07 \times 10^{-18}$ for Ch. 8 (upper right in (e)) and 2.04×10^{-78} for Ch. 9 (lower left in (e))]. Averages and standard deviations of waveforms are taken from 100 trials.

2 mm (initial gap, 0% strain) to ≈3 mm (50% strain at 3.3 mN). Although the film's strain causes 3D deformation of each beam, which results in a gap between the Pt electrode and the tissue surfaces, the gap can be filled with a conductive solution of saline, and each electrode site detects signals of the tissue via the saline (Supporting Information).

These Pt electrodes enable the ECoG signals ranging from alpha to high-gamma oscillations (8–100 Hz) to be detected (Figure 3e). During physical whisker stimulation (an electromagnetic vibrator for the mouse whiskers, Supporting Information), the Ch. 8 electrode, which was positioned over the S1B, detected the neuronal activities with an amplitude of 154 $\mu V_{p\text{-}p}$ and a peak time of 54.2 ms. These waveforms are similar to the ECoG signals recorded by conventional ECoG electrodes,[15] suggesting that these signals evoked neuronal responses by the stimuli [$p = 1.07 \times 10^{-18}$, $n = 100$ trials, by paired t-test between prestimulus (–200 to 0 ms) and poststimulus (0 to 200 ms) periods]. While visually stimulating the mouse using a light source [a white light-emitting diode array, stimulation duration of 500 ms, Supporting Information], the other electrode (Ch. 9) placed over the V1 detected neuronal activities with an amplitude of 667 $\mu V_{p\text{-}p}$ and a peak time of 80.6 ms, suggesting that these signals are significantly evoked neuronal responses by the stimuli [$p = 2.04 \times 10^{-78}$, $n = 100$ trials, by paired t-test between prestimulus (–200 to 0 ms) and poststimulus (0 to 200 ms) periods]. Waveforms recorded by the Ch. 9 electrode during whisker stimulation (Figure 3e, lower right waveform) [$p = 4.54 \times 10^{-4}$, $n = 100$ trials, by paired t-test between prestimulus (–200 to 0 ms) and poststimulus (0 to 200 ms) periods] is thought not to be caused by the device crosstalk associated with the parasitic impedance of the device interconnections (250 times larger impedance than the Ch. 9 electrode's impedance). In addition, the waveform of Ch. 9 is not similar to the Ch. 8 electrode's one. The waveform is probably due to the volume conduction or local spread of activity around the S1B.[17]

Figure 3e also includes the time-frequency domain plots for both ECoG signals. The time-frequency domain plots taken from S1B (Ch. 8) show that physical stimulation to the mouse whiskers increases the ECoG power in the 8–60 Hz frequency band, but visual stimulation has a negligible impact on the ECoG power. The other time-frequency domain plots of the ECoG signals from V1 (Ch. 9) show that the ECoG power in 8–100 Hz from V1 (Ch. 9) responds to visual stimulation, but not whisker stimulation. These results indicate that the ECoG signals with tunable Pt electrodes using the Kirigami design show reasonable stimulus selectivity in each cortical region.

Another challenge for flexible bioprobe film devices is applying them to organs that show large and rapid changes in the volume and the surface area (e.g., a beating heart). Due to the deformable property of the heart, the strain-force required to stretch the film device should be minimized to follow the natural deformations while beating. **Figure 4**a,b shows a fabricated 5 × 91 slits design film device wrapped around a beating mouse heart. During a heartbeat, the film device stretches following large and rapid (≈2.5 cycle s^{-1}) changes in the volume and the surface area of the heart (Movie S4 of the Supporting Information).

With a Kirigami device consisting of an array of 10-channel planar Pt electrodes (50 μm diameter, ≈300 kΩ impedance at 1 kHz), we demonstrated epicardial electrocardiogram (ECG) signal recordings from the beating mouse heart. Such an epicardial ECG recording can map the heart with a high spatial resolution. An array of Pt electrodes, Chs. 1–5, was placed over the ventricle side of the heart, while the other array of Chs. 6–10 was placed over the atrium side (Figure 4b, Chs. 1, 2, 9, and 10 are not visible in the photograph). Figure 4c–f shows the signals detected via the Ch. 7 electrode; atrial beats are observed without the ventricular beats. Figure 4c,d are the recorded signals for the whole recording period of 0–1200 s and the early period of 0–50 s, respectively. Neither shows a significant change in the amplitude of the ECGs during the recording (≈4 mV_{pp} in amplitude). Figure 4e show the signal waveforms in the early recording period of 0–2 s and the later period of 1000–1002 s, respectively. Figure 4f shows superimposition of these recorded waveforms across a low threshold voltage of –1.5 mV; these waveforms are well superimposed. For further analysis of the waveforms, an one-way analysis of variance (ANOVA) test was performed on the period from –0.02–0.10 s (red dashed line area in Figure 4f) to confirm the stability of the ECG recording. The ANOVA shows that the effect of the time difference during the ECG recording is vanishingly small compared to the amplitude of the waveforms, indicating that the Kirigami bioprobe device stably recorded ECG signals from the beating heart ($F_{2929,\ 8751910} = 208930.68$, $p < 0.0001$).

Herein we demonstrate that a Kirigami-based parylene film has a great stretchability that exceeds 1000% (Figure 1). We also propose metal layer embedded Kirigami bioprobe devices with the high stretchabilities: ≈250% at 9 mN and a Young's modulus of 23 kPa (maximum device strain of ≈470% at 65 mN) for the 5 × 91-slit device and a Young's modulus of 3.6 kPa (maximum strain of ≈840%) for the 3 × 91-slit device (Figure 2j). This device can record neuronal signals from the cerebral cortex with a tunable electrode gap (Figure 3) and can stably record from a dynamically deformed organ (Figure 4; Movie S4 of the Supporting Information). Although the Kirigami films in both recording applications require a stretchability of <50% (Figures 3 and 4), the additional stretchability (strain) should realize other applications, including detection of growth of brain plaques and Alzheimer's disease. An ontogenetic process and pathological hypertrophy/atrophy of a brain tissue cause deformations >300%.[5] However, conventional stretchable devices using elastic materials cannot realize a sufficient stretchability to follow the organ's deformation.[2,3] In addition, conventional stretchable devices require a large force to stretch the films, resulting in a force-induced stress to the organ that prevents natural deformation and growth. As demonstrated in the animal experiments, the Kirigami design can significantly reduce the force required to stretch film devices, enabling minimally invasive neuronal recordings.

Because numerous biological tissues and organs show biaxial deformations, such bioprobe film devices must be biaxially stretchable. The slit pattern (or the width/length of the thin film beam) determines the stretching properties of the film itself, including both the spring constant and the stretching direction. Besides fabricating a set of slit patterns, which realizes the one-directional stretching property of the film (Figure 1), we also

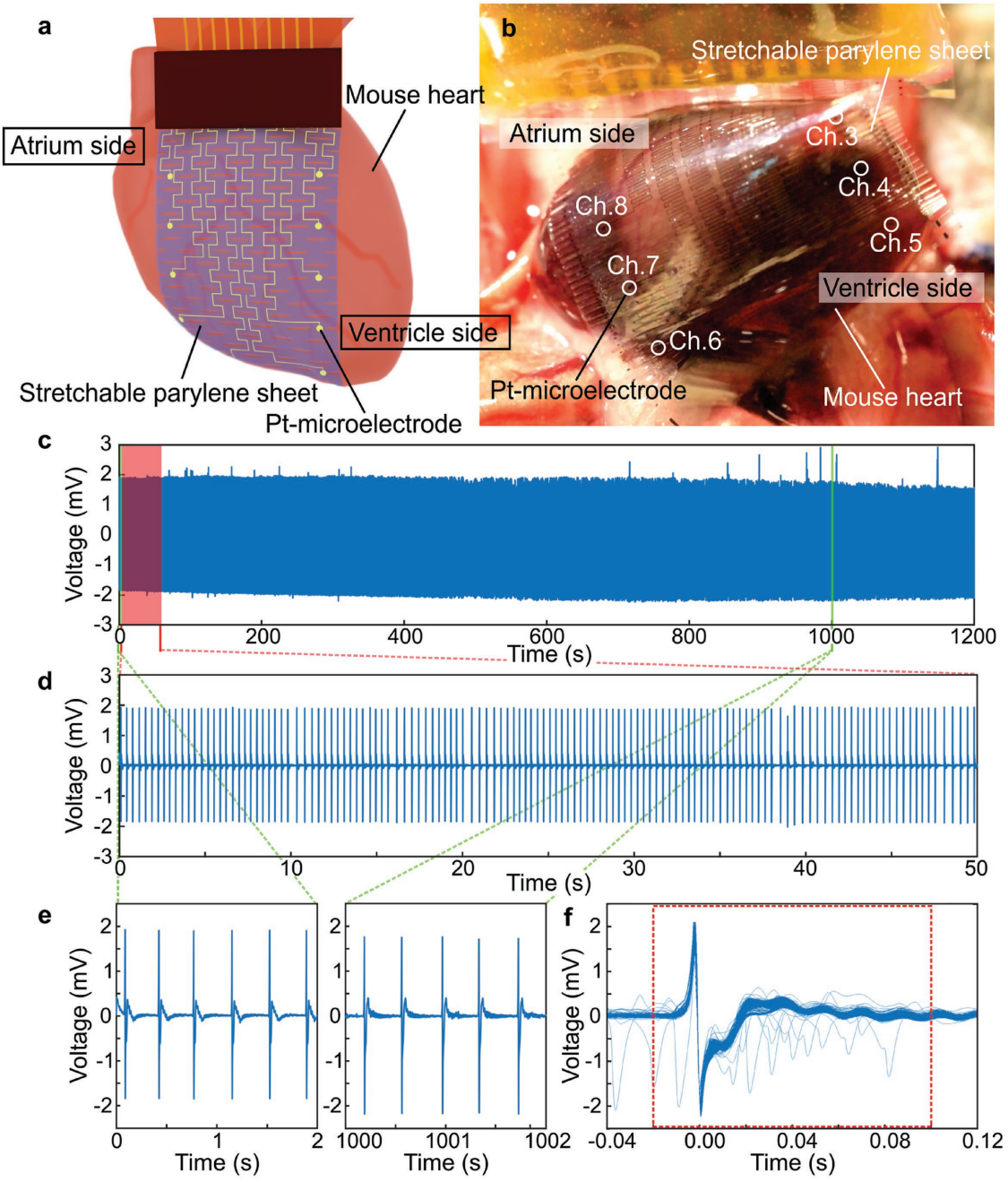

Figure 4. ECG signal recordings from a mouse heart in vivo. a,b) Schematic and photograph of the fabricated device [5 × 91 slits design ($N_r = 5$, $N_c = 45$)] wrapped around a beating mouse heart in vivo (also see Movie S4 of the Supporting Information). Sets of Pt electrodes of Chs. 1–5 and Chs. 6–10 are placed over the ventricle side and atrium side of the heart, respectively. c) Epicardial ECG signals detected via the electrode Ch. 7, which is placed on the atrium side of the heart. d) Recorded ECG signals for the early period of 0–50 s. e) Signal waveforms in the early period of 0–2 s and the later period of 1000–1002 s during the recording for 1200 s. f) Superimposition of recorded waveforms recorded for the whole period of 1200 s (the number of waveforms, 2988). Red dashed square is consistent with the period used for ANOVA test.

fabricated a parylene film with the two-directional slit pattern, and demonstrated "biaxial" stretchability by placing the film over a rubber balloon (Figure S8 of the Supporting Information). Compared to the one-directional slit pattern for uniaxial stretchability, the two-directional slit pattern occupies a larger area in the film (Figure S8 of the Supporting Information), resulting in a limited area for the microscale electrode array and the interconnections. Improvements of the device design such as multilayered interconnections (> two metal layers) and thinner interconnection widths (<20 μm) are necessary to embed a large number of electrode channels in a biaxial film. Herein we show a preliminary biaxial device. However, the concept of a biaxially stretchable Kirigami device will enhance opportunities for numerous biaxially stretching samples, including the tongue, trapezius muscle, and thoracic diaphragm.

The demonstrated bioprobe film device consists of microscale planar Pt electrodes, enabling both ECoG and ECG signals to be detected. Such microscale electrodes can also be used for electrically stimulating sites,[18] enhancing the performance of the film device in electrophysiological studies. Although we demonstrated biological signal recordings using a passive electrode array (50 μm diameter planar Pt electrodes), embedding flexible field effect transistor (FET)-based circuitry into the parylene membrane is also possible using flexible materials, including carbon nanotubes,[19] semiconducting nanowires,[20] nanomembranes,[21,22] InGaZnO,[23,24] and poly(3,4-ethylenedioxythiophene): poly(styrenesulfonate) (PEDOT: PSS).[25] Because the stretchability of a Kirigami device is based on the bending of each membrane of parylene, embedding flexible FETs into the membrane may realize Kirigami-based active film devices with a high stretchability.

In conclusion, we propose highly stretchable, deformable, and flexible film bioprobe devices by simply patterning slits as a Kirigami design. Because the stretchability of the film obeys the slit design (or the beam geometry) and the material properties of the beam, a film with numerous strain-force characteristics can be designed for specific applications. With a Kirigami-designed parylene film, we fabricated highly stretchable electrode devices (≈250% at 9 mN, maximum stretchability of 470%), and demonstrated biological signal recordings from the brain tissue and heart of a mouse, confirming the device's advantages: tunable electrode gaps over the brain and wrapping around a beating heart. In these animal experiments where the film stretches <50%, the required forces to strain these films are <3.3 mN. Consequently, the Kirigami design significantly reduces the film's strain-force compared to conventional stretchable electronics using elastomer substrates. Such a reduction is an important characteristic for stretchable film electronics, particularly in devices attached to soft samples such as heart or brain tissue.

We also propose that the highly stretchable bioprobe film device is applicable to tissues and organs exhibiting time-dependent increases and decreases in the surface and the volume due to growth or disease. Employing the film's high stretchability, new classes of device applications requiring a high stretchable film with a smaller strain-force may be realized, including medical tools, wearable devices, sensors, actuators, and energy harvesters.

Experimental Section

All experimental procedures using animals were approved by the committees for the use of animals at Toyohashi University of Technology, and all animal care followed the Standards Relation to the Care and Management of Experimental Animals (Notification No. 6, March 27, 1980 of the Prime Minister's Office of Japan).

Supporting Information

Supporting Information is available from the Wiley Online Library or from the author.

Acknowledgements

Y.M., S.Y., and H.S. contributed equally to this work. This work was supported by Grants-in-Aid for Scientific Research (A) (Grant No. 25249047), (B) (Grant No. 17H03250), for Young Scientists (A) (Grant No. 26709024), the PRESTO Program from JST, and Strategic Advancement of Multi-Purpose Ultra-Human Robot and Artificial Intelligence Technologies program from NEDO. Y.M. was supported by the Leading Graduate School Program R03 of MEXT. R.N. was also supported by Takeda Science Foundation.

Conflict of Interest

The authors declare no conflict of interest.

Keywords

flexible devices, kirigami, neural recording, stretchable devices

Received: September 18, 2017
Published online:

[1] T. Sekitani, Y. Noguchi, K. Hata, T. Fukushima, T. Aida, T. Someya, *Science* **2008**, *321*, 1468.
[2] N. Matsuhisa, M. Kaltenbrunner, T. Yokota, H. Jinno, K. Kuribara, T. Sekitani, T. Someya, *Nat. Commun.* **2015**, *6*, 7461.
[3] S. Xu, Y. Zhang, J. Cho, J. Lee, X. Huang, L. Jia, J. A. Fan, Y. Su, J. Su, H. Zhang, H. Cheng, B. Lu, C. Yu, C. Chuang, T.-I. Kim, T. Song, K. Shigeta, S. Kang, C. Dagdeviren, I. Petrov, P. V. Braun, Y. Huang, U. Paik, J. A. Rogers, *Nat. Commun.* **2013**, *4*, 1543.
[4] D. E. Discher, *Science* **2005**, *310*, 1139.
[5] O. Kapellou, S. J. Counsell, N. Kennea, L. Dyet, N. Saeed, J. Stark, E. Maalouf, P. Duggan, M. Ajayi-Obe, J. Hajnal, J. M. Allsop, J. Boardman, M. A. Rutherford, F. Cowan, A. D. Edwards, *PLoS Med.* **2006**, *3*, 1382.
[6] K. Khanafer, A. Duprey, M. Schlicht, R. Berguer, *Biomed. Microdevices* **2009**, *11*, 503.
[7] R. J. Lang, in *Proc. 12th Annu. Symp. Comput. Geom.—SCG '96*, ACM, Philadelphia, PA, USA **1996**, p. 98.
[8] M. K. Blees, A. W. Barnard, P. a. Rose, S. P. Roberts, K. L. McGill, P. Y. Huang, A. R. Ruyack, J. W. Kevek, B. Kobrin, D. a. Muller, P. L. McEuen, *Nature* **2015**, *524*, 204.
[9] T. C. Shyu, P. F. Damasceno, P. M. Dodd, A. Lamoureux, L. Xu, M. Shlian, M. Shtein, S. C. Glotzer, N. A. Kotov, *Nat. Mater.* **2015**, *14*, 785.
[10] S. Sosin, T. Zoumpoulidis, M. Bartek, L. Wang, R. Dekker, K. M. B. Jansen, L. J. Ernst, in *Proc. Electron. Components Technol. Conf.*, IEEE, Lake Buena Vista, FL, USA **2008**, p. 1339.
[11] S. Yamagiwa, M. Ishida, T. Kawano, *Appl. Phys. Lett.* **2015**, *107*, 1.
[12] S. Yamagiwa, M. Ishida, T. Kawano, in *Proc. IEEE Int. Conf. Micro Electro Mech. Syst.*, IEEE, Taipei, Taiwan **2013**, p. 480.
[13] M. Isobe, K. Okumura, *Sci. Rep.* **2016**, *6*, 24758.
[14] D.-H. Kim, J. Viventi, J. J. Amsden, J. Xiao, L. Vigeland, Y.-S. Kim, J. A. Blanco, B. Panilaitis, E. S. Frechette, D. Contreras, D. L. Kaplan, F. G. Omenetto, Y. Huang, K.-C. Hwang, M. R. Zakin, B. Litt, J. A. Rogers, *Nat. Mater.* **2010**, *9*, 511.
[15] H. Toda, T. Suzuki, H. Sawahata, K. Majima, Y. Kamitani, I. Hasegawa, *Neuroimage* **2011**, *54*, 203.
[16] B. Rubehn, C. Bosman, R. Oostenveld, P. Fries, T. Stieglitz, *J. Neural Eng.* **2009**, *6*, 36003.
[17] D. H. Lim, M. H. Mohajerani, J. LeDue, J. Boyd, S. Chen, T. H. Murphy, *Front. Neural Circuits* **2012**, *6*, 11.
[18] S. Yamagiwa, A. Fujishiro, H. Sawahata, R. Numano, M. Ishida, T. Kawano, *Sens. Actuators, B* **2015**, *206*, 205.
[19] D. Sun, M. Y. Timmermans, Y. Tian, A. G. Nasibulin, E. I. Kauppinen, S. Kishimoto, T. Mizutani, Y. Ohno, *Nat. Nanotechnol.* **2011**, *6*, 156.
[20] K. Takei, T. Takahashi, J. C. Ho, H. Ko, A. G. Gillies, P. W. Leu, R. S. Fearing, A. Javey, *Nat. Mater.* **2010**, *9*, 821.

[21] J. Viventi, D. Kim, L. Vigeland, E. S. Frechette, J. A. Blanco, Y. Kim, A. E. Avrin, V. R. Tiruvadi, S. Hwang, A. C. Vanleer, D. F. Wulsin, K. Davis, C. E. Gelber, L. Palmer, J. Van Der Spiegel, J. Wu, J. Xiao, Y. Huang, D. Contreras, J. A. Rogers, B. Litt, N. America, *Nat. Neurosci.* **2011**, *14*, 1599.

[22] J. Viventi, D.-H. Kim, J. D. Moss, Y.-S. Kim, J. A. Blanco, N. Annetta, A. Hicks, J. Xiao, Y. Huang, D. J. Callans, J. A. Rogers, B. Litt, *Sci. Transl. Med.* **2010**, *2*, 24ra22.

[23] K. Nomura, H. Ohta, A. Takagi, T. Kamiya, M. Hirano, H. Hosono, *Nature* **2004**, *432*, 488.

[24] K. Nomura, A. Takagi, T. Kamiya, H. Ohta, M. Hirano, H. Hosono, *Jpn. J. Appl. Phys., Part 1* **2006**, *45*, 4303.

[25] D. Khodagholy, T. Doublet, P. Quilichini, M. Gurfinkel, P. Leleux, A. Ghestem, E. Ismailova, T. Hervé, S. Sanaur, C. Bernard, G. G. Malliaras, *Nat. Commun.* **2013**, *4*, 1575.